Electronic Supplementary Material (ESI) for Molecular Systems Design & Engineering.

Supporting information

Hydrazone-based hole transporting material prepared *via* condensation chemistry as alternative for cross-coupling chemistry for perovskite solar cells

Michiel L. Petrus,[1]†* Maximilian T. Sirtl,[1]† Anna C. Closs,[1] Thomas Bein, [1] Pablo Docampo[2,*]

[1] Department of Chemistry and Center for NanoScience (CeNS), University of Munich (LMU) Butenandtstr. 11, 81377 Munich, Germany

[2] Newcastle University, School of Electrical and Electronic Engineering, NE1 7RU Newcastle upon Tyne, UK

† These authors contributed equally to this work

* e-mail: michiel.petrus@lmu.de, pablo.docampo@newcastle.ac.uk

Methods

General characterization techniques. UV-Vis spectra were recorded using a Perkin Elmer Lambda 1050 spectrometer with an integrating sphere**.** FTIR were obtained using a Perkin Elmer FT-Infrared Spectrometer Paragon 1000. ^{1}H- and ^{13}C-NMRspectra were recorded using a Bruker spectrometer Avance III HD 400 MHz. All spectra where referenced to the solvent (^{1}H-NMR: $CDCl_3$ δ = 7.26 ppm; ^{13}C-NMR: $CDCl_3$ δ = 77.0 ppm). HRMS measurements were carried out using a Thermo Finnigan MAT 95.

Cyclic voltammetry (CV). Cyclic voltammetry experiments were performed using a Metrohm Potentiostat (PGSTAT302N) with platinum working and counter electrode and an Ag/AgCl reference electrode. Experiments were performed in anhydrous and degassed dichloromethane solutions of the hole transporter with 0.1 M tetrabutylammonium hexafluorophosphate (tBuNPF6) as electrolyte and a scan rate of 100 mV s^{-1}. HOMO levels were calculated according to literature with the formal potential of the Fc^{+}/Fc redox positioned at −5.1 eV vs. vacuum.[1]

Thermal characterization. Thermogravmetric analysis (TGA) was performed using a Netzsch STA 449 C Jupiter under nitrogen atmosphere with a scan rate of 10 °C min^{-1}. Differential scanning calorimetry (DSC) was performed under nitrogen atmosphere using a Perkin Elmer DSC8000 at a heating rates in the range of 10–50 °C min^{-1}. Melting behavior was confirmed using a melting point apparatus.

Powder X-ray diffraction (PXRD). Powder X-ray diffraction analysis of HTM crystal structures was carried out in transmission mode using a STOE Stadi PM diffractometer with Cu $K\alpha_1$-radiation (λ = 1.5406 Å) operating at 40 kV and 40 mA, equipped with a DECTRIS MYTHEN 1 K solid-state strip detector.

Preparation $MAPbI_3$ and FAMACs devices:

Substrate etching and cleaning

All chemicals were purchased from Sigma Aldrich unless stated otherwise. Fluorine-doped tin oxide (FTO) coated glass substrates (Pilkington TEC 7) were patterned and then etched with 2 M HCl and zinc powder. Substrates were

scrubbed with detergent (2% Hellmanex in water) and then washed with water, acetone and ethanol. The FTO was treated in oxygen plasma for 5 min immediately prior to the spin-coating the electron transporting layer.

Electron transport layer deposition

A compact TiO_2 layer was prepared from a sol-gel precursor solution by spincoating onto the freshly prepared substrates for 45 s at 2000 rpm. The substrates were afterwards calcinated at 500 °C for 30 min at air. For the sol-gel solution a 2 M solution of HCl in dry 2-propanol was added dropwise to a vigorously stirring 0.43 mM solution of Ti-isopropoxide (99.999 %) in dry 2-propanol.

FAMACs perovskite precursor solution and film deposition

1.5 M $Cs_{0.05}(FA_{0.83}MA_{0.17})_{0.95}Pb(I_{0.83}Br_{0.17})_3$ with excess lead iodide was prepared with 215 mg FAI, 28 mg MABr (Dyesol), 634 mg PbI_2 (TCI), and 92 mg $PbBr_2$ (TCI). A 1.875 M solution of CsI in DMSO was then diluted into the precursor solution. The perovskite solution was prepared in a mixture of anhydrous DMF (800 µL) and DMSO (200 µL) and stirred in nitrogen atmosphere on a hot plate at 70 °C for 15. After filtration, the room temperature precursor solution was deposited on FTO/TiO_2 substrates in a nitrogen filled glove box and spin-coated at 1000 rpm for 10 s and then at 6000 rpm for 20 s (ramp of 2000 rpm s^{-1}). 500 µL of chlorobenzen was quickly dispensed onto the substrate 10 s before the end of spin-coating, and then the substrate was annealed on a hot plate at 100 °C for 45 min. After deposition of the HTM, the films were stored at < 30 % relative humidity overnight.

$MAPbI_3$ perovskite precursor solution and film deposition

For the $MAPbI_3$ precursor solution methylammonium iodide (Dyesol; 0.2 g; 1.25 mmol) and PbI_2 (TCI, >98%; 0.61 g; 1.3 mmol) were dissolved in *N,N*-dimethylformamide (DMF) : dimethyl sulfoxide (DMSO) solvent mixture (1:4 vol/vol; 1 mL) under stirring at 100 °C. The solution was spin-coated dynamically (80 µL; first at 1000 rpm for 10 s, followed by a second step at 5000 rpm for 30 s) onto the substrate. After 20 s, chlorobenzene (400 µL) was added on top of the spinning substrate and afterwards the substrate was annealed on a hotplate (first at 40 °C for 40 min, followed by a second step at 100 °C for 10 min). After deposition of the HTM, the films were stored at < 30 % relative humidity over night.

Hole transport layer and electrode deposition FAMACs and $MAPbI_3$ devices

The hole transport material (HTM) 2,2',7,7'-tetrakis(N,N'-di-p-methoxyphenylamine)-9,9'-spirobifluorene (spiro-OMeTAD) was prepared by dissolving 75 mg spiro-OMeTAD (Borun chemicals) in 1 mL anhydrous chlorobenzene. To this solution 30 µL of a lithium bis(trifluoromethanesulfonyl)imide (Li-TFSI) solution (170 mg mL^{-1}in acetonitrile) and 10 µL tert-butylpyridine (tBP) were added. 80 µL of this solution was spincoated dynamically onto the substrate at 1500 rpm.

For the deposition on FAMACs, to 20 mg of EDOT-MPH 800 µL anhydrous chlorobenzene and 200 µL anhydrous chloroform along with 10 µL tBP and 20 µL of a Li-TFSI solution (170 mg mL^{-1} in acetonitrile) were added. The mixture was heated at 60 °C for 5-10 minutes until the solution became transparent, and was then passed through a Chromafil 0.45 µm PET-45/15 MS syringe filter while hot. The filtered solution was left on a hot plate at 40 °C while spin-coating. 80 µL of the EDOT-MPH solution was quickly dispensed onto the substrates while they were spinning at 1000 rpm for 45 s.

For deposition on $MAPbI_3$. To 15 mg of EDOT-MPH 800 µL anhydrous chlorobenzene and 200 µL anhydrous chloroform along with 10 µL tBP and 20 µL of a Li-TFSI solution (170 mg mL^{-1} in acetonitrile) were added. The mixture was heated at 80 °C for 5-10 minutes until the solution became transparent, and was then passed through a Chromafil 0.45 µm PET-45/15 MS syringe filter while hot. The filtered solution was left on a hot plate at 60 °C while spin-coating. 80 µL of the EDOT-MPH solution was quickly dispensed onto the substrates while they were spinning at 1000 rpm for 45 s.

The substrates were left in a desiccator box for 24 h for the HTM to oxidize before thermally evaporating a 50 nm gold electrode under vacuum of < 9 x 10^{-6} mbar.

Solar cell characterization

J/V-curves of solar cells were recorded under ambient conditions under simulated AM 1.5 sunlight, with an incident power of approximately 100 mW cm-2, which was corrected for the exact light intensity using a Fraunhofer ISE certified silicon cell. The active area of the solar cells was defined with a square metal aperture mask of 0.0831 cm^2.

The reported device characteristics were estimated from the measured *J/V*-curves obtained from the reverse scan (from V_{OC} to J_{SC}) which was recorded at a scan rate of 0.2 V s-1 after pre-biasing at 1.5 V for 5 s under illumination using a Newport OrielSol 2A solar simulator with a Keithley 2401 source meter. All as-prepared devices show a comparable degree of hysteresis between the forward and reverse scan.

Charge transport measurements

Hole-only device preparation and characterization. ITO-substrates (1.5 x 2.0 cm, VisionTek, 12 Ω/sq to 15 Ω/sq) were etched and cleaned. The substrates were plasma cleaned prior to the thermal deposition of the MoO_x layer (10 nm) under vacuum (~$1 \cdot 10^{-6}$ mbar). The substrates were exposed to air and stored in a nitrogen-filled glovebox. Next, the EDOT-MPH was spincoated from a chlorobenzene:chloroform mixture as described above at a concentration of 10 mg mL^{-1}. A top electrode of MoO_x (10 nm), followed by a layer of gold (40 nm) was deposited under vacuum (~$1 \cdot 10^{-6}$ mbar). The active area of the device was 0.16 cm^2. Current-voltage characteristics were recorded in air in the dark using a Metrohm potentiostat (PGSTAT302N) at a scan rate of 0.1 V s^{-1}. The layer thickness which was around 50 nm was determined for the individual films by using atomic force microscopy (AFM) measurements, which were performed in tapping mode using a NanoInk DPN Stage microscope, or with a Veeco Dektak 150.

Conductivity device preparation and characterization. Glass substrates with a thin compact layer of Al_2O_3 were used to improve the wetting of the HTMs on the substrate. EDOT-MPH was spincoated at 1000 rpm from a chloroform:chlorobenzene mixture as described above containing the given amount of LiTFSI as oxidant, resulting in a film thickness of approximately 50 nm. The films allowed to oxidize for 24 h in a desiccator at a relative humidity < 30 %. 40 nm thick gold electrodes were thermally deposited under vacuum (~10^{-6} mbar). The electrode pattern was designed for two point probe measurements with a channel length of 250, 500 and 1000 µm, a channel width of 0.2, 0.1 and 0.056 m respectively. No significant differences were observed depending on the electrode pattern and the measured values were averaged over at least 8 individual devices. *JV*-curves were recorded under ambient conditions without illumination using a Keithley 2400 source meter at a scan rate of 1 V s^{-1} in the range from -5 to 5 V.

Computational study. The geometry optimization and electronic structure calculations were carried out using Gaussian09 program package. Density functional theory (DFT) geometry optimizations using the B3LYP/6-31G(d,p) basis set were performed in vacuum and in dichloromethane as the solvent, by means of the conductor-like polarizable continuum model (CPCM). The calculated HOMO energy level was obtained by adding 0.624 eV to the HOMO energy level obtained from DFT calculations using DCM as solvent.[2]

Synthetic details

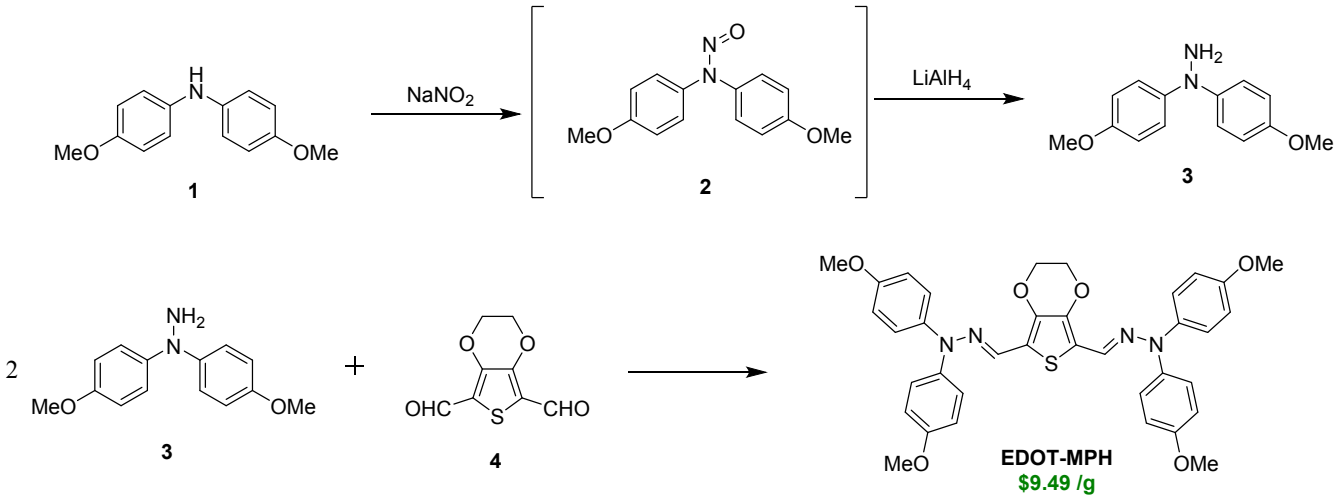

Scheme S1 | Synthesis of EDOT-MPH and its starting material.

Synthesis of 1,1-Bis(methoxyphenyl)amine (1)

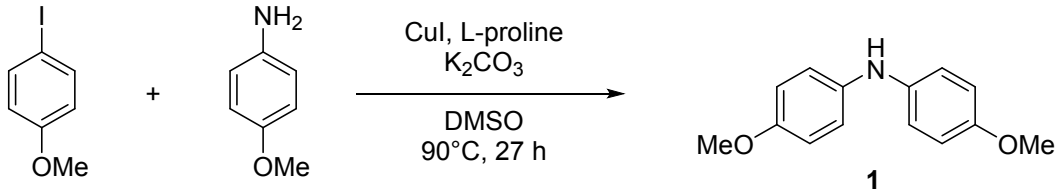

A mixture of K_2CO_3 (17.44 g, 125 mmol, 2 eq), CuI (1.22 g, 6.29 mmol, 0.1 eq) and L-proline (1.47 mg, 12.58 mmol, 0.2 eq) was added to a solution of 4-Iodoanisole (1.8 g, 62.9 mmol, 1 eq) DMSO (150 mL), resulting in a black color. *p*-anisolidine, (12.8 g, 103.8 mmol, 1.5 eq) was added, and the mixture stirred at 90 °C for 2 days. After filtration of the suspension, the solution was extracted with ethyl acetate (3 x 200 mL). The combined organic layers were washed with brine and dried with Na_2SO_4. After filtration the solvent was removed *in vacuo* and the product was recrystallized from diethyl ether. After a short silica-

column (Eluent: Ethyl acetate/hexane 7:1), the product was obtained as red-orange crystals in a yield of 52 %.

^{1}H-NMR ($CDCl_3$, 400 MHz): δ= 6.934 (d_t, 4 H, *J*= 8.8 Hz), 6.827 (d_t, 4 H, *J*= 8.8 Hz), 5.249 (s, 1 H), 3.784 (s, 6 H) ppm.

Characterization in agreement with literature.[3]

Synthesis of *N,N*-bis(4-mothoxyphenyl)nitrous amide (2)

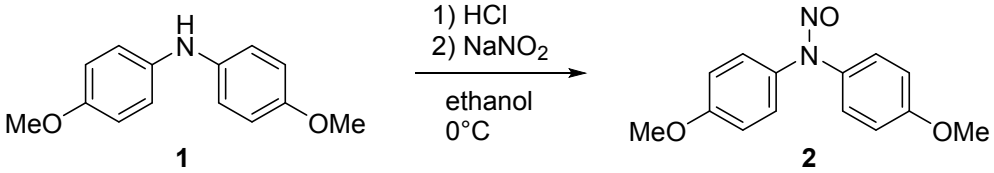

1 **2**

HCl (37 %, 20 mL) was added to a solution of Bis(4-methoxyphenyl)amine (5 g, 21.8 mmol, 1 eq in 120 mL ethanol) at 0°C and and the orange solution was stirred vigorously for 5 min. To this mixture, 50 mL of a 0.47 M solution of $NaNO_2$ in water was added dropwise, leading to a white precipitate which was formed immediately. After stirring at 0 °C for 1 h, the product was filtered off as a colorless powder and dried *in vacuo*. The product was obtained in a good yield of 91 % and stored in the glovebox.

^{1}H-NMR ($CDCl_3$, 400 MHz): δ= 7.332 (d_t, 2 H, *J*= 8.8 Hz), 7.076–7.033 (m, 6 H), 3.795 (d, 6 H) ppm.

^{13}C-NMR ($CDCl_3$, 100 MHz): δ= 159.51, 158.48, 135.50, 129.74, 128.35, 122.19, 114.91, 114.67, 55.48, 55.44 ppm.

Characterization in agreement with literature.[4]

Synthesis of 1,1-bis(4-methoxyphenyl)hydrazine (3)

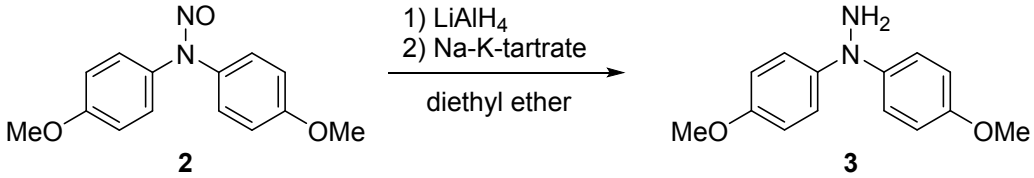

2 **3**

To a solution of the as received nitrous amide **2** (5 g, 19.37 mmol, 1 eq in 300 mL diethyl ether), $LiAlH_4$ (1 g, 26.2 mmol, 1.4 eq in 40 mL diethyl ether) was added dropwise, leading to an off-white suspension which was stirred for 2 h at room temperature. After the careful addition of a saturated Na-K-tartrate solution in water, the organic layer was extracted with diethyl ether (3 x 150 mL). HCl (37 %) was added to the combined organic layers, resulting in a white precipitation of the product. After addition of a 0.75 M NaOH solution (50 mL in water), the product was extracted with diethyl ether (3 x 150 mL) and the combined organic layers were dried with $MgSO_4$. The solvent was removed *in vacuo* and the product was obtained as a red crystalline powder in a medium yield of 58.4 %.

^{1}H-NMR ($CDCl_3$, 400 MHz): δ= 7.074 (d_t, 4 H, *J*= 8.8 Hz), 6.839 (d_t, 4 H, *J*= 9.2 Hz), 4.046 (s, 2 H), 3.790 (s, 6 H) ppm.

Characterization in agreement with literature.[4]

Synthesis of EDOT-MPH (5)

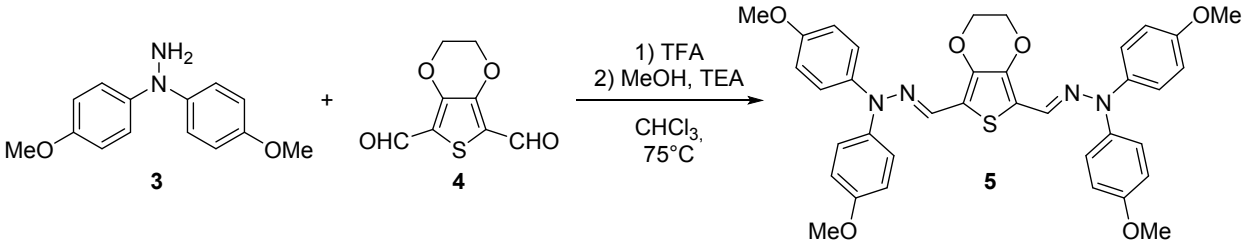

To the red solution of **3** (0.33 g, 1.35 mmol, 2.3 eq) in 10 mL dry chloroform, compound **4** (0.12 eq, 0.59 mmol, 1 eq)[5] was added, together with one drop of trifluoro acetic acid. After the mixture was stirred over night at room temperature, it was heated to reflux for 4 hours. After cooling down, the product was crushed out by adding 50 mL methanol. After the addition of 0.1 mL triethylamine in order to neutralize the suspension, the product was filtered off a bright orange powder and washed with methanol. The product was dried under vacuum and obtained in a high yield of 97 %. The workup was performed under ambient conditions.

^{1}H-NMR ($CDCl_3$, 400 MHz): δ= 7.218 (s, 2 H), 7.103 (d_t, 4 H, *J*= 8.8 Hz), 6.946 (d_d, 4 H, *J*= 8.8 Hz), 4.086 (s, 4 H), 3.831 (s, 12 H) ppm.

^{13}C-NMR ($CDCl_3$, 100 MHz): δ= 156.60, 139.12, 137.33, 126.31, 123.55, 115.47, 115.05, 64.77, 55.61 ppm.

HRMS (FAB^+) m/z: $[M]^+$ calculated for $C_{36}H_{34}O_6N_4S$: 650.2199; found: 650.2224

FTIR: *ν*(cm^{-1}): 3050 (vw), 3000 (w), 2927 (w), 2831 (w), 1602 (m, **C=N-N**), 1548 (w), 1500 (vs), 1435 (s), 1368 (s), 1299 (m), 1244 (vs), 1199 (vs), 1112 (s), 1065 (vs), 952 (s), 816 (vs).

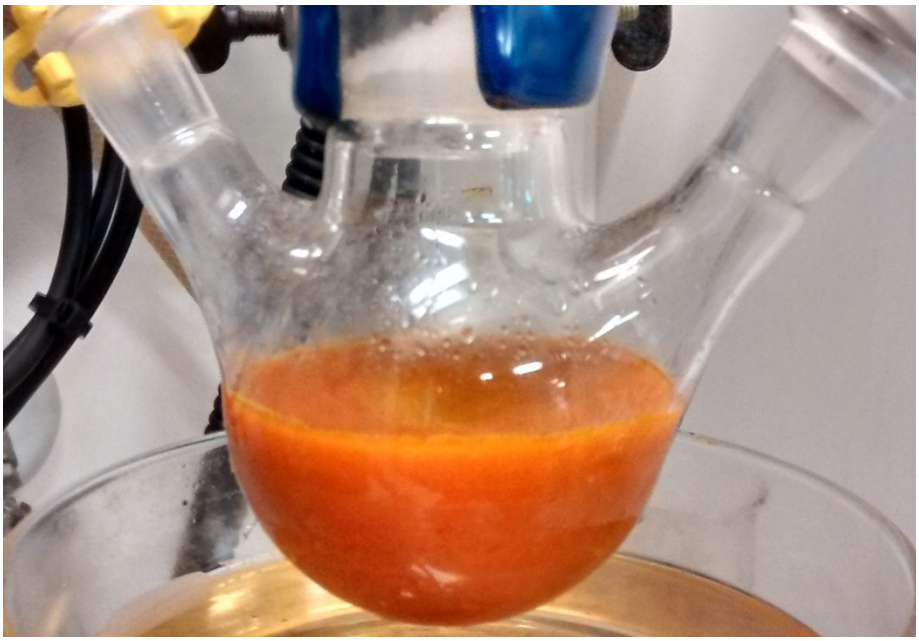

Figure S1 | **Crude product.** Reaction vessel showing the bright orange product right before filtering it off.

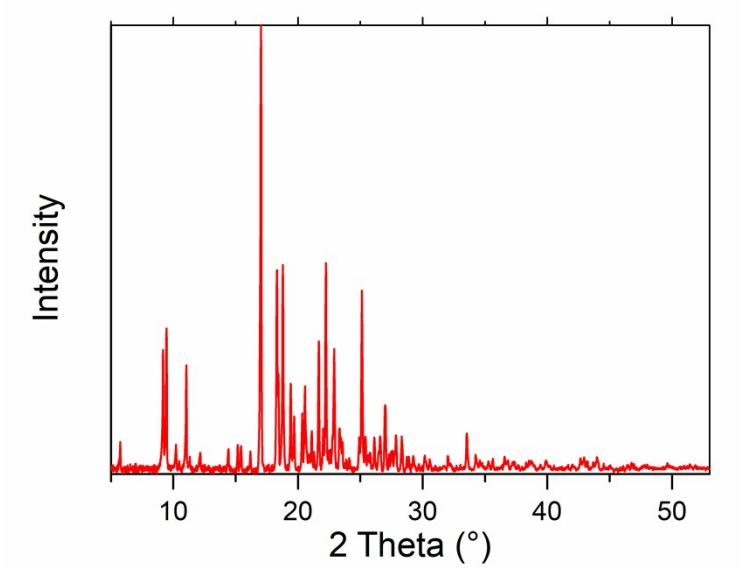

Figure S2 | **PXRD patterns of pristine EDOT-MPH**, demonstrating that the material is crystalline.

Cost Estimation

In order to make an estimate of the cost of the different hole transporting materials, we used the cost model as was described by Osedach et al. [7] which was implemented by ourselves for HTMs for perovskite solar cells. [5,6] For every synthetic step the required amounts of reactants, catalysts, reagents and solvents are calculated to obtain 1 gram of the final product. Additionally, the required materials for workup and purification were estimated using the procedure as published.

1. Quenching/neutralization. The required amounts were evaluated on a case-by-case basis. For neutralization a stoichiometric amount of the acid or base were assumed to be necessary.

2. Extraction: The use of 150 mL solvent (three times 50 mL) and 1 gram of drying agent (Na_2SO_4 or $MgSO_4$) were assumed to be required to obtain 1 gram of the (intermediate) product.

3. Recrystallization. We assume that 1 gram of product requires 100 mL of solvent and that the procedure is only performed once.

4. Distillation/sublimation. We assume no chemicals are required and no chemical waste, the energy was similar to other steps not included.

5. Washing. We assume 100 mL of solvent is required to wash 1 gram of the (intermediate) product.

6. Filtering. We assume 50 mL of solvent is required to filter 1 gram of the (intermediate) product.

The quantities are based on published procedures where the synthesis, workup and purification are performed on a lab scale. Upscaling to a multi-kilogram scale might reduce the quantities, especially materials used in the purification, considerably. For example, multiple steps could possibly be combined to reduce the number of isolation steps (“telescoping”). Further, solvents might be replaced for cheaper (and/or environmentally friendly) alternatives or reused to reduce materials and waste cost. For this reason, the estimated material cost could be seen as an upper limit.

The starting materials and therefore the amount of synthetic steps could be a topic of debate, however most of the used starting materials are common starting materials for the different synthetic routes. In example, 4-iodoaniline has been used as starting material just like in previous published work.

In order to estimate the cost, quotes (for bulk quantities when possible) have been collected from major chemical suppliers (Sigma-Aldrich, Acros Organics and Fischer Chemicals) for all used chemicals. The costs were multiplied by the quantities that are required for the synthesis and the sum of all costs was calculated to estimate to total material cost.

Different synthetic routes were evaluated in order to find the most cost effective route. We found that especially procedures that require column chromatography for purification add significantly to the cost, as a result of the high prices of silica gel together with the large amounts of solvent used. Also upscaling of column chromatography to a multi-kilogram scale will be challenging.

Furthermore, production on a large scale could have an influence on the price of starting materials. The cost of starting materials might be reduced significantly. Also by finding other suppliers of chemicals the cost of (especially organic) starting materials could be further reduced. In example, 3,4-ethylenedioxythiophene (EDOT) is commercially available at Sigma- Aldrich and Acros organics in small quantities at prices exceeding $5,000 per kilogram, while other suppliers offer the same material in an even higher purity in bulk quantities at prices below $250 per kilogram.

We also note that the material cost only takes into account the cost of materials used. Equipment, energy consumption, maintenance, waste treatment, lab space, profit and various other overhead charges are not taken into account. Depending on the synthesis and purification steps, this could also have a significant influence on the cost. For example, palladium cross-coupling reactions require stringent conditions, making the upscaling significant more costly than simple reactions that can be performed at ambient conditions. In the case of pharmaceutical drugs, for example, the materials cost accounts for only 20-45% of the total cost of drug synthesis.

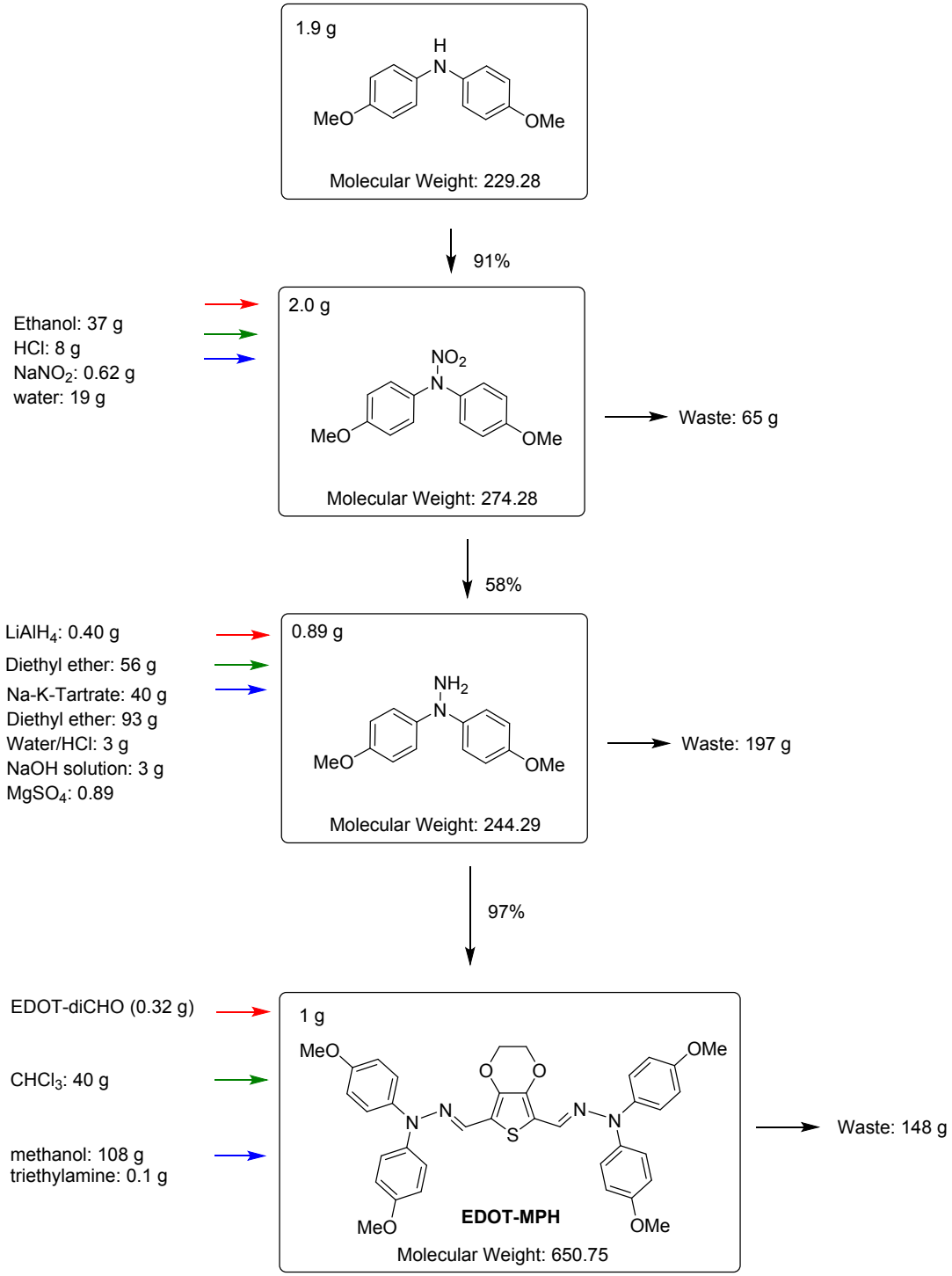

Scheme S2 | Synthesis scheme for cost estimation and chemical waste.

Table S1 | Cost analysis and overall cost for the synthesis of 1 g EDOT-MPH.

Chemical	Weight reagent (g)	Weight solvent (g)	Weight workup (g)	Total weight		Chemical cost ($/kg)	Cost ($/g product)	Cost ($/step)
Amine	1.9			1.9		$1,666.00	$3.17	$3.32
Ethanol		37		37		$3.16	$0.12	
HCl		8		8		$3.39	$0.03	
$NaNO_2$		0.62		0.62		$17.12	$0.01	
Water		19		19		$0.00	$0.00	
$LiAlH_4$	0.4			0.4		$522.80	$0.21	$4.48
DEE		56		56		$22.89	$1.28	
Na-K-Tartrate			40	40		$19.46	$0.78	
DEE			93	93		$22.89	$2.13	
HCl			3	3		$3.39	$0.01	
NaOH			3	3		$7.56	$0.02	
MgSO4			0.89	0.89		$54.24	$0.05	
EDOT	0.32			0.32		4262.36	$1.36	$1.69
TFA	0.02			0.02		$141.12	$0.00	
chloroform		40		40		$2.60	$0.10	
methanol			108	108		$1.98	$0.21	
triethylamine			0.1	0.1		$23.18	$0.00	
Total	**3**	**160**	**248**	**411**				**$9.49**

Thermal Properties

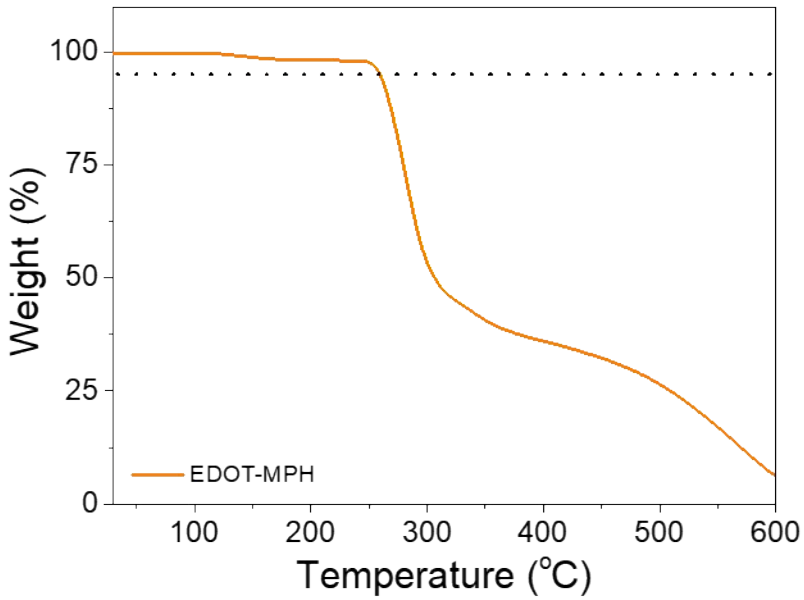

Figure S3 | **TGA thermogram of EDOT-MPH** recorded under nitrogen atmosphere with a heating rate of 10 °C/min. The dotted black line indicates the 5% weight loss.

Geometry optimization

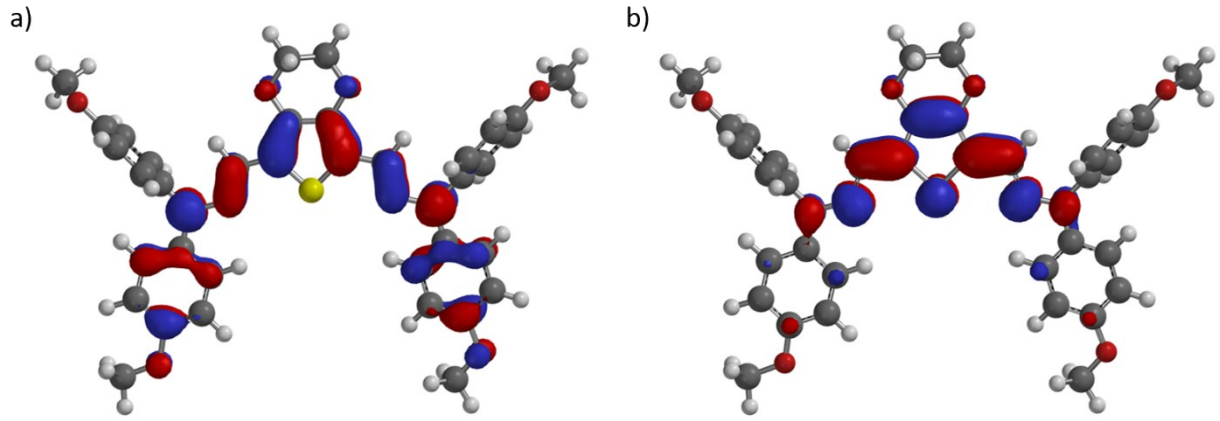

Figure S4 | **Frontier molecular orbital distributions.** Distribution of the HOMO (a) and LUMO (b) levels, obtained from DFT calculations in vacuum.

Charge carrier mobility

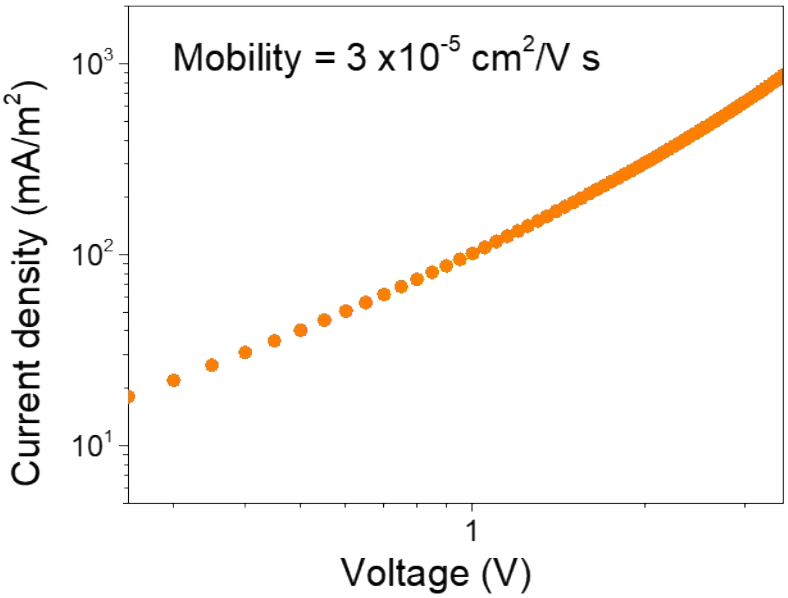

Figure S5 | ***J-V* curves of single "hole-only" devices.** Device architecture: ITO)/MoO_x/EDOT-MPH/MoO_x/Au. The mobility was obtained by fitting the equation for space-charge limited current.

Photovoltaic performance

Doping of the hole-transporting materials

We wish to point out that it is difficult to compare the amount of LiTFSI that is used for preparing the different HTM layers, as the concentration of the solutions is different. The amount of LiTFSI that was added to the solution for spincoating was optimized in order to obtain the best PCE in devices. The concentration of LiTFSI in the EDOT-MPH solution is lower, but due to the low concentration and different molecular weight the relative concentration in equivalents is slightly higher than for Spiro-OMeTAD. In detail:

For EDOT-MPH, 20 µL of a 170 mg/mL LiTFSI solution was added to a 20 mg/mL EDOT-MPH solution. This results in a final concentration of 1.2×10^{-2} mmol LiTFSI/mL, and 40 mol% LiTFSI relative to EDOT-MPH. For Spiro-OMeTAD, 30 µL of a 170 mg/mL LiTFSI solution was added to a 75 mg/mL Spiro-OMeTAD solution. This results in a final concentration of 1.8×10^{-2} mmol LiTFSI/mL, and 30 mol% LiTFSI relative to Spiro-OMeTAD.

The amount and ratio of LiTFSI in the final HTM film might again change as a result of the different film deposition conditions used to prepare the HTM layer. While the amount of oxidized HTM, which again is influence by the permeation of oxygen, will also play a role."

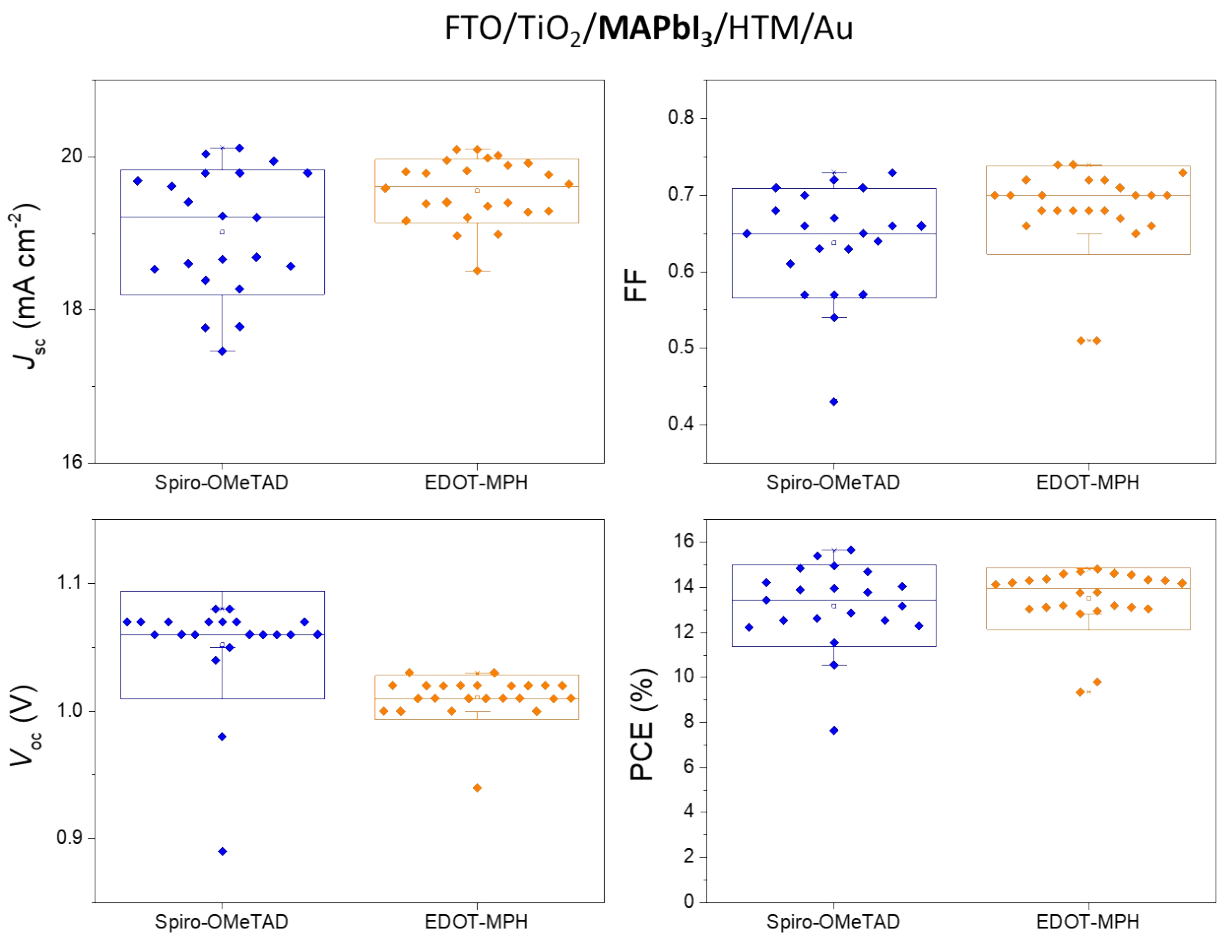

Figure S6 | **Photovoltaic performance $MAPbI_3$ devices**. Box-plot of 45 individual devices prepared showing the comparison of the photovoltaic parameters of devices comprising either EDOT-MPH or Spiro-OMeTAD as HTM. Device architecture: FTO/TiO_x/$MAPbI_3$/HTM/Au.

Table S2 | **Overview statistical analysis of 45 individual $MAPbI_3$ devices**

	dF	T stat	P (T<=t) two-tail	T critical two tail
J_{sc}	29	2.74	0.010	2.05
V_{oc}	26	-4.14	0.0003	2.06
FF	39	2.21	0.033	2.02
PCE	37	0.68	0.501	2.03

Null hypothesis: the photovoltaic parameters for devices comprising EDOT-MPH and Spiro-OMeTAD are the same. If T stat > T critical we can conclude that, with a certainty of 95%, the null-hypothesis for the given parameter is not true (meaning the improvement is significant). dF is the degrees of freedom (number closely related to the sample size). The P-value determines the statistical significance (should not be confused with the error rate).

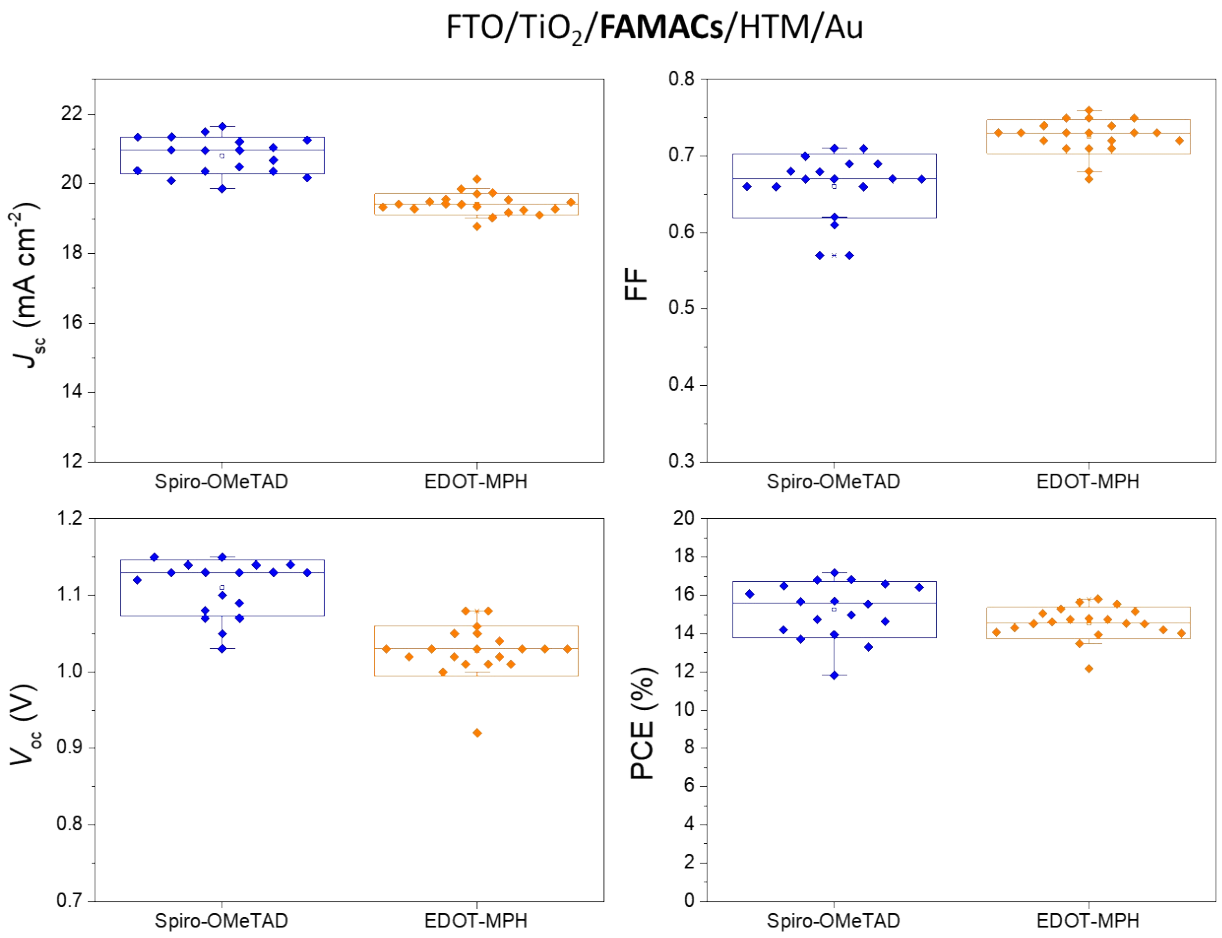

Figure S7 | **Photovoltaic performance FAMACs devices**. Box-plot of 38 individual devices prepared showing the comparison of the photovoltaic parameters of devices comprising either EDOT-MPH or Spiro-OMeTAD as HTM. Device architecture: FTO/TiO_x/FAMACs/HTM/Au.

Table S3 | **Overview statistical analysis of 38 individual FAMACs devices**

	dF	T stat	P (T<=t) two-tail	T critical two tail
J_{sc}	27	-9.88	1.8×10^{-10}	2.05
V_{oc}	35	-7.25	1.8×10^{-8}	2.03
FF	25	5.86	4.1×10^{-6}	2.06
PCE	26	-1.79	0.086	2.06

Null hypothesis: the photovoltaic parameters for devices comprising EDOT-MPH and Spiro-OMeTAD are the same. If T stat > T critical we can conclude that, with a certainty of 95%, the null-hypothesis for the given parameter is not true (meaning the improvement is significant). dF is the degrees of freedom (number closely related to the sample size). The P-value determines the statistical significance (should not be confused with the error rate).

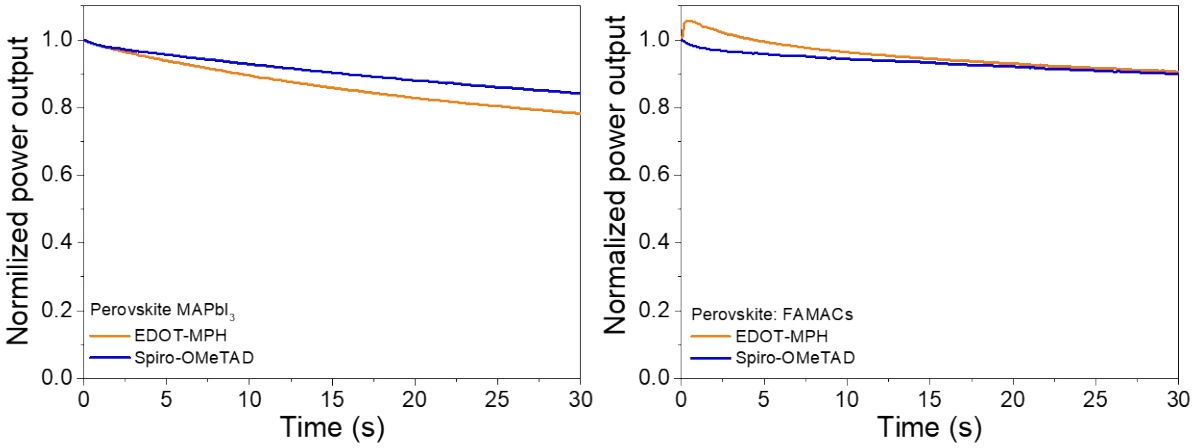

Figure S8 | **Stabilized power output curves** of the photovoltaic devices comprising the different HTMs in combination with the different perovskite absorber.

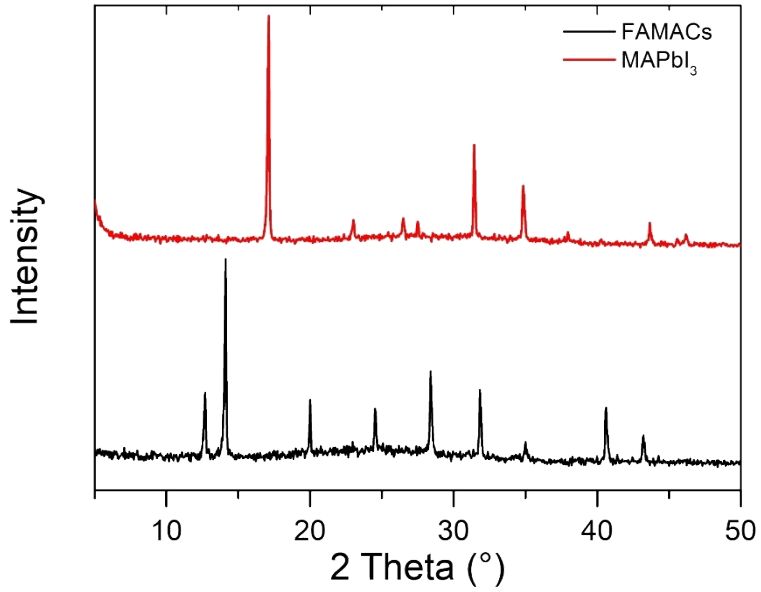

Figure S9 | **XRD patterns of the pristine perovskites ($MAPbI_3$ and FAMACs)** used as active area in solar cells and measures in film.

Charge carrier lifetime

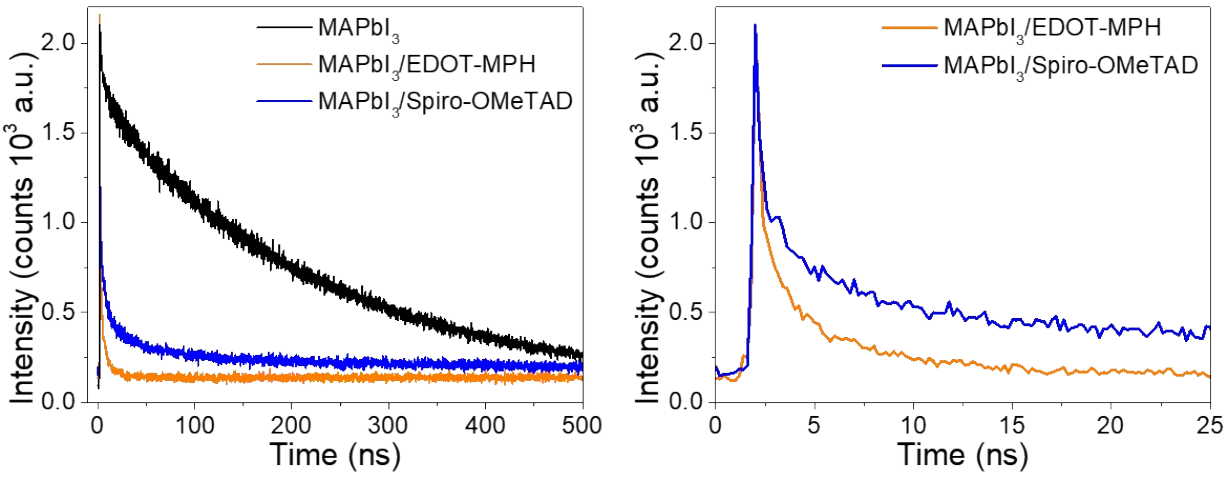

Figure S10 | Time resolved photoluminescence decay of $MAPbI_3$ films and bilayers consisting of $MAPbI_3$/HTM, obtained for the same amount of counts.

References:

1 C. C. M., L. Wei, K. A. E., S. David and B. G. C., *Adv. Mater.*, 2011, **23**, 2367–2371.

2 W.-J. Chi, Q.-S. Li and Z.-S. Li, *Nanoscale*, 2016, **8**, 6146–6154.

3 D. Ma, Q. Cai and H. Zhang, *Org. Lett.*, 2003, **5**, 2453–2455.

4 I. A. Tonks, A. C. Durrell, H. B. Gray and J. E. Bercaw, *J. Am. Chem. Soc.*, 2012, **134**, 7301–7304.

5 M. L. Petrus, T. Bein, T. J. Dingemans and P. Docampo, *J. Mater. Chem. A*, 2015, **3**, 12159–12162.

6 M. L. Petrus, A. Music, A. C. Closs, J. C. Bijleveld, M. T. Sirtl, Y. Hu, T. J. Dingemans, T. Bein and P. Docampo, *J. Mater. Chem. A*, 2017, **5**, 25200–25210.

7 T. P. Osedach, T. L. Andrew and V. Bulović, *Energy Environ. Sci.*, 2013, **6**, 711–718.